roughly 300 animals, and given a choice between an optimal concentration of benzaldehyde (1:200 dilution in ethanol) and a lower concentration of diacetyl (1:10,000 dilution in ethanol) in the presence of a uniform field of butanone (1.2 μl per 10-ml plate). Under these conditions more than 95% of wild-type animals prefer benzaldehyde. Animals that accumulated at the diacetyl source were removed and retested under the same conditions to repeat the enrichment. Animals that preferred diacetyl three times were isolated, and their F_3 broods were given a choice between benzaldehyde and diacetyl in the absence of a uniform concentration of butanone. Mutants that could chemotax to benzaldehyde under these conditions were saved. Twenty-seven mutants exhibited discrimination defects that could also be replicated without the diacetyl counterattractant. Mutants were backcrossed twice to wild-type animals.

Genetic mapping of *ky542*

We mapped *ky542* to chromosome II by observing segregation of the discrimination phenotype away from the dominant marker *sqt-1(sc1)* (7/7 isolates). Subsequent mapping was performed by following segregation of the discrimination phenotype with single-nucleotide polymorphisms (SNPs) between the wild-type N2 and CB4856 strains. F_2 progeny of *ky542* × CB4856 crosses were isolated, and populations were generated from each isolate. Each population was tested for butanone/benzaldehyde discrimination. Populations that were homozygous mutant and those that were homozygous wild type were retained, whereas populations that appeared to be heterozygous were discarded. We isolated DNA from each population, and scored SNPs by polymerase chain reaction amplification followed by restriction-enzyme digestion. Using 33 populations, we found that *ky542* mapped between SNPs located on cosmid C01F1 (chromosome II, position −4.5) and cosmid C34F1 (chromosome II, position −2.5).

Laser ablations

AWC neurons were ablated in a wild-type strain that contained an integrated *str-2::GFP* reporter (*kyIs140*) at the L1 or L2 larval stage[17]. The AWC neuron was identified by its characteristic position or by the use of the *str-2::GFP* marker, and then laser irradiated. Ablation was confirmed for AWC^{ON}-ablated animals by looking for *str-2::GFP* expression after all assays had been performed. Single-animal assays were performed on gravid adults as early as the second day after ablation and as late as the fourth day. We assayed the same animals on two or three consecutive days. As many as three consecutive olfactory assays were performed in a single day. For discrimination assays, in which animals were challenged with the same attractant in the presence and absence of saturating odour, animals were allowed to recover between tests for 1 h on a fresh plate with no odours. The order of the assays was randomized on different days. Single-animal assay plates were poured 1 day before the assays and allowed to air dry for 1 h before the assays.

Received 6 November 2000; accepted 11 January 2001.

1. Bargmann, C. I., Hartwieg, E. & Horvitz, H. R. Odorant-selective genes and neurons mediate olfaction in *C. elegans*. *Cell* **74,** 515–527 (1993).
2. Troemel, E. R., Sagasti, A. & Bargmann, C. I. Lateral signaling mediated by axon contact and calcium entry regulates asymmetric odorant receptor expression in *C. elegans*. *Cell* **99,** 387–398 (1999).
3. Sengupta, P., Chou, J. H. & Bargmann, C. I. *odr-10* encodes a seven transmembrane domain olfactory receptor required for responses to the odorant diacetyl. *Cell* **84,** 899–909 (1996).
4. Troemel, E. R., Chou, J. H., Dwyer, N. D., Colbert, H. A. & Bargmann, C. I. Divergent seven transmembrane receptors are candidate chemosensory receptors in *C. elegans*. *Cell* **83,** 207–218 (1995).
5. Troemel, E. R. *Chemosensory Receptors in Caenorhabditis elegans.* Ph.D. Thesis, Univ. California (1999).
6. L'Etoile, N. D. & Bargmann, C. I. Olfaction and odor discrimination are mediated by the *C. elegans* guanylyl cyclase ODR-1. *Neuron* **25,** 575–586 (2000).
7. Komatsu, H., Mori, I., Rhee, J.-S., Akaike, N. & Ohshima, Y. Mutations in a cyclic nucleotide-gated channel lead to abnormal thermosensation and chemosensation in *C. elegans*. *Neuron* **17,** 707–718 (1996).
8. Coburn, C. M. & Bargmann, C. I. A putative cyclic nucleotide-gated channel is required for sensory development and function in *C. elegans*. *Neuron* **17,** 695–706 (1996).
9. Roayaie, K., Crump, J. G., Sagasti, A. & Bargmann, C. I. The G alpha protein ODR-3 mediates olfactory and nociceptive function and controls cilium morphogenesis in *C. elegans* olfactory neurons. *Neuron* **20,** 55–67 (1998).
10. Birnby, D. A., Link, E. M., Vowels, J. J., Tian, H., Colacurcio, P. L. & Thomas, J. H. A transmembrane guanylyl cyclase (DAF-11) and Hsp90 (DAF-21) regulate a common set of chemosensory behaviors in *Caenorhabditis elegans*. *Genetics* **155,** 85–104 (2000).
11. Chou, J. H., Bargmann, C. I. & Sengupta, P. The *Caenorhabditis elegans odr-2* gene encodes a novel Ly-6-related protein required for olfaction. *Genetics* **157,** 211–224 (2001).
12. Weinshenker, D., Wei, A., Salkoff, L. & Thomas, J. H. Block of an ether-a-go-go-like K^+ channel by imipramine rescues *egl-2* excitation defects in *Caenorhabditis elegans*. *J. Neurosci.* **19,** 9831–9840 (1999).
13. Sengupta, P., Colbert, H. A. & Bargmann, C. I. The *C. elegans* gene *odr-7* encodes an olfactory-specific member of the nuclear receptor superfamily. *Cell* **79,** 971–980 (1994).
14. Pierce-Shimomura, J. T., Faumont, S., Gaston, M. R., Pearson, B. J. & Lockery S. R. The homeobox gene *lim-6* is required for distinct chemosensory representations in *C. elegans*. *Nature* **410,** 694–698 (2001).
15. Troemel, E. R., Kimmel, B. E. & Bargmann, C. I. Reprogramming chemotaxis responses: sensory neurons define olfactory preferences in *C. elegans*. *Cell* **91,** 161–169 (1997).
16. Brenner, S. The genetics of *Caenorhabditis elegans*. *Genetics* **77,** 71–94 (1974).
17. Bargmann, C. I. & Horvitz, H. R. Chemosensory neurons with overlapping functions direct chemotaxis to multiple chemicals in *C. elegans*. *Neuron* **7,** 729–742 (1991).

Acknowledgements

We thank A. Sagasti and N. L'Etoile for for discussions and insights into AWC asymmetry; H. Nguyen for technical assistance; S. Wicks and R. Plasterk for sharing unpublished data; C. Adler and S. Kirch for advice on microscopy; and A. Sagasti, S. Shaham, N. L'Etoile, J. Gray and C. Adler for comments on the manuscript. P.D.W. was supported by a postdoctoral fellowship from the Jane Coffin Childs Memorial Fund for Medical Research. C.I.B. is an Investigator of the Howard Hughes Medical Institute. This work was supported by a grant from the National Institutes of Health.

Correspondence and requests for materials should be addressed to C.I.B. (e-mail: cori@itsa.ucsf.edu).

Bone marrow cells regenerate infarcted myocardium

Donald Orlic†, Jan Kajstura*, Stefano Chimenti*, Igor Jakoniuk*, Stacie M. Anderson†, Baosheng Li*, James Pickel‡, Ronald McKay‡, Bernardo Nadal-Ginard*, David M. Bodine†, Annarosa Leri* & Piero Anversa*

* *Department of Medicine, New York Medical College, Valhalla, New York 10595, USA*
† *Hematopoiesis Section, Genetics and Molecular Biology Branch, NHGRI, and* ‡ *Laboratory of Molecular Biology, NINDS, NIH, Bethesda, Maryland 20892, USA*

Myocardial infarction leads to loss of tissue and impairment of cardiac performance. The remaining myocytes are unable to reconstitute the necrotic tissue, and the post-infarcted heart deteriorates with time[1]. Injury to a target organ is sensed by distant stem cells, which migrate to the site of damage and undergo alternate stem cell differentiation[2–5]; these events promote structural and functional repair[6–8]. This high degree of stem cell plasticity prompted us to test whether dead myocardium could be restored by transplanting bone marrow cells in infarcted mice. We sorted lineage-negative (Lin^-) bone marrow cells from transgenic mice expressing enhanced green fluorescent protein[9] by fluorescence-activated cell sorting on the basis of c-*kit* expression[10]. Shortly after coronary ligation, Lin^- c-kit^{POS} cells were injected in the contracting wall bordering the infarct. Here we report that newly formed myocardium occupied 68% of the infarcted portion of the ventricle 9 days after transplanting the bone marrow cells. The developing tissue comprised proliferating myocytes and vascular structures. Our studies indicate that locally delivered bone marrow cells can generate *de novo* myocardium, ameliorating the outcome of coronary artery disease.

Injection of male Lin^-c-kit^{POS} bone marrow cells (see Supplementary Information) in the peri-infarcted left ventricle of female mice resulted in myocardial regeneration. Repair was obtained in 12 out of 30 mice (40%). Failure to reconstitute infarcts was attributed to the difficulty of transplanting cells into tissue contracting at 600 beats per minute. However, an immunological reaction to the histocompatibility antigen on the Y chromosome of the donor bone marrow cells could account for the lack of repair in some of the female recipients. Closely packed myocytes occupied 68 ± 11% of the infarcted region and extended from the anterior to the posterior aspect of the ventricle (Fig. 1a–d). The fraction of endocardial and epicardial circumference delimiting the infarcted area[1,11] did not differ in untreated mice, 78 ± 18% ($n = 8$), or in mice treated with Lin^-c-kit^{POS} cells, 75 ± 14% ($n = 12$), or Lin^-c-kit^{NEG}cells, 75 ± 15% ($n = 11$). New myocytes were not found in mice injected with Lin^-c-kit^{NEG}cells (Fig. 1e).

The origin of the cells in the forming myocardium was deter-

© 2001 Macmillan Magazines Ltd

mined by the expression of enhanced green fluorescent protein (EGFP) (Fig. 2; see also Supplementary Information) and the presence of Y chromosome (Supplementary Information). EGFP was restricted to the cytoplasm, whereas Y chromosome was restricted to the nuclei of new cardiac cells. EGFP and Y chromosome were not detected in the surviving portion of the ventricle. EGFP expression was combined with the labelling of proteins specific for myocytes, endothelial cells and smooth muscle cells. This allowed us to identify each cardiac cell type, and to recognize endothelial and smooth muscle cells organized in coronary vessels (Fig. 3a–c; see also Supplementary Information). The percentage of new myocytes, endothelial cells and smooth muscle cells expressing EGFP was $53 \pm 9\%$ ($n = 7$), $44 \pm 6\%$ ($n = 7$) and $49 \pm 7\%$ ($n = 7$), respectively. These values were consistent with the fraction of transplanted Lin$^-$c-*kit*^{POS} bone marrow cells that expressed EGFP, $44 \pm 10\%$ ($n = 6$). An average $54 \pm 8\%$ ($n = 6$) of myocytes, endothelial cells and smooth muscle cells expressed EGFP in the heart of donor transgenic mice.

To confirm that newly formed myocytes represented maturing cells aiming at functional competence, we examined expression of the myocyte enhancer factor 2 (MEF2), the cardiac specific transcription factor GATA-4 and the early marker of myocyte development Csx/Nkx2.5. In the heart, MEF2 proteins are recruited by GATA-4 to activate synergistically the promoters of several cardiac genes, such as myosin light chain, troponin T, troponin I, α-myosin heavy chain, desmin, atrial natriuretic factor and α-actin[12,13]. Csx/Nkx2.5 is a transcription factor restricted to the initial phases of

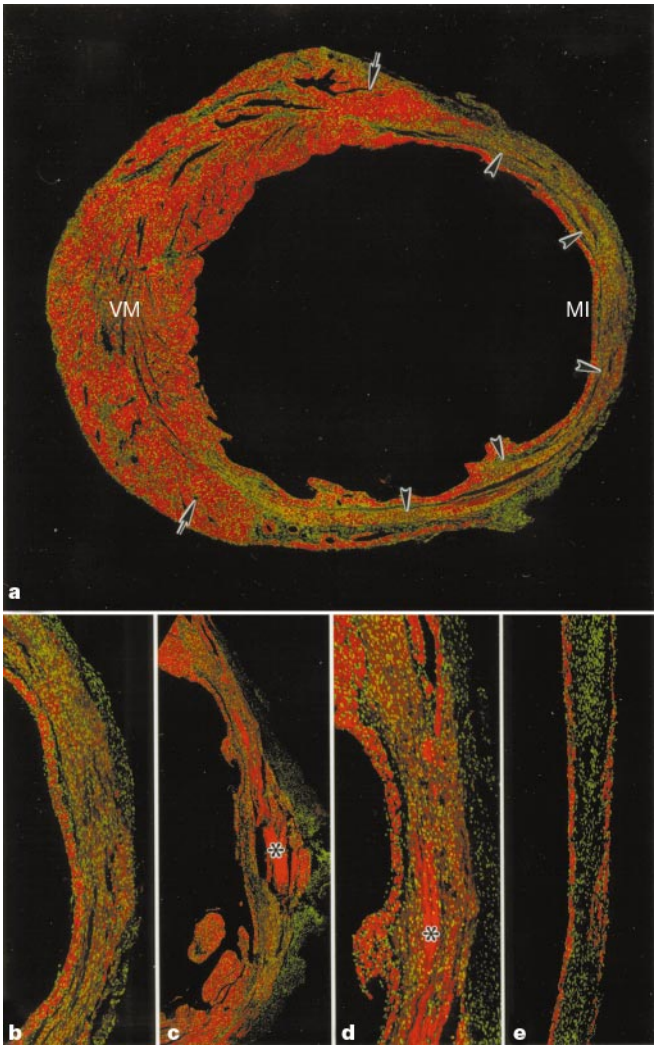

Figure 1 Bone marrow cells and myocardial regeneration. **a**, Myocardial infarct (MI) injected with Lin$^-$ c-*kit*^{POS} cells from bone marrow (arrows). Arrowheads indicate regenerating myocardium; VM, viable myocardium. **b**, Same MI at higher magnification. **c**, **d**, Low and high magnifications of MI injected with Lin$^-$c-*kit*^{POS} cells. **e**, MI injected with Lin$^-$ c-*kit*^{NEG} cells; only healing is apparent. Asterisk indicates necrotic myocytes. Red, cardiac myosin; green, propidium iodide labelling of nuclei. Original magnification, ×12 (**a**); ×25 (**c**) ×50 (**b**, **d**, **e**).

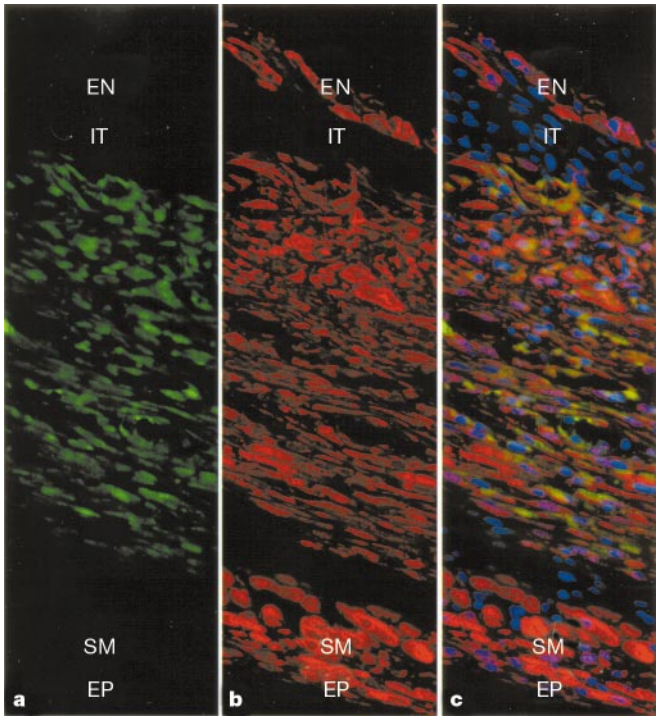

Figure 2 Myocardial infarct injected with Lin$^-$c-*kit*^{POS} cells; myocardium is regenerating from endocardium (EN) to epicardium (EP). **a**, EGFP (green); **b**, cardiac myosin (red); **c**, combination of EGFP and myosin (red–green), and propidium-iodide-stained nuclei (blue). Infarcted tissue (IT) can be seen in the subendocardium, spared myocytes (SM) can be seen in the subepicardium. Original magnification, ×250 (**a**–**c**).

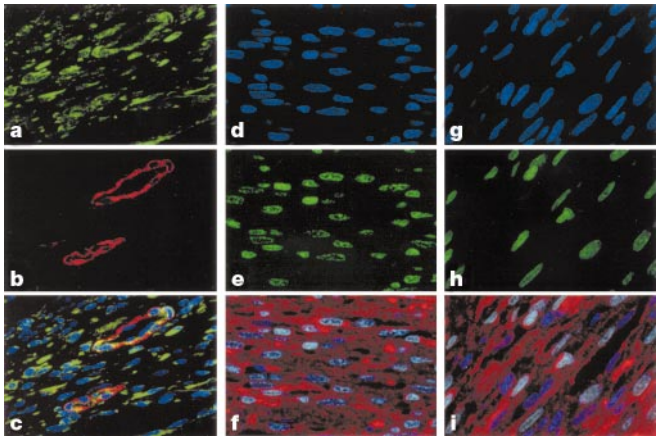

Figure 3 Regenerating myocardium in myocardial infarct injected with Lin$^-$ c-*kit*^{POS} cells. **a**, EGFP (green); **b**, smooth muscle α-actin in arterioles (red); **c**, combination of EGFP and smooth muscle α-actin (yellow–red), and propidium iodide (PI)-stained nuclei (blue). **d**–**i**, MEF2 and Csx/Nkx2.5 in cardiac myosin-positive cells. **d**, **g**, PI-stained nuclei (blue); **e**, **h**, MEF2 and Csx/Nkx2.5 labelling (green); **f**, **i**, cardiac myosin (red), and combination of MEF2 or Csx/Nkx2.5 with PI (bright fluorescence in nuclei). Original magnification, ×300 (**a**–**i**).

© 2001 Macmillan Magazines Ltd

myocyte differentiation[12]. In the reconstituting heart, all nuclei of cells labelled with cardiac myosin expressed MEF2 (Fig. 3d–f) and GATA-4 (Supplementary Information), but only 40 ± 9% expressed Csx/Nkx2.5 (Fig. 3g–i).

To characterize further the properties of these myocytes, we determined the expression of connexin 43. This protein is responsible for intercellular connections and electrical coupling through the generation of plasma-membrane channels between myocytes[14,15]; connexin 43 was apparent in the cell cytoplasm and at the surface of closely aligned differentiating cells (Fig. 4). These results were consistent with the expected functional competence of the heart muscle phenotype. In addition, myocytes at various stages of maturation were detected within the same and different bands (Fig. 5).

Ki67 is expressed in cycling cells in G1, S, G2 and early mitosis[16], providing a quantitative estimate of the fraction of cells in the cell cycle at the time of observation. 5-Bromodeoxyuridine (BrdU) labelling identifies nuclei in S phase[16,17]; therefore, we injected BrdU for 4–5 days to assess cumulative cell division during active growth (Supplementary Information). Proliferation of myocytes was 93% ($P < 0.001$) and 60% ($P < 0.001$) higher than that of endothelial cells, and 225% ($P < 0.001$) and 176% ($P < 0.001$) higher than that of smooth muscle cells, when measured by BrdU and Ki67, respectively (BrdU: myocytes 36 ± 8%; endothelial cells 19 ± 5%; smooth muscle cells 11 ± 2%; Ki67: myocytes 19 ± 3%; endothelial cells 12 ± 3%; smooth muscle cells 7 ± 2%; $n = 8$ in all cases). Dividing myocytes were small with partially aligned myofibrils, resembling late fetal/neonatal cells; 40–50% of the Ki67- or BrdU-positive cells expressed EGFP.

Cell differentiation caused a loss of c-*kit* surface receptors. We observed only two undifferentiated cells showing c-*kit* on the cell membrane in the subendocardium of the infarcted wall. These c-*kit*-labelled cells were in proximity but not within the regenerating band. They expressed EGFP, confirming their origin from the transplant (Supplementary Information).

To determine whether developing myocytes derived from the Lin$^-$c-*kit*^{POS} cells had an impact on function, we obtained haemodynamic parameters before death. Results from infarcted mice non-injected or injected with Lin$^-$c-*kit*^{NEG}cells were combined. In comparison with sham-operated mice, the infarcted groups exhibited indices of cardiac failure (Fig. 6a). In mice treated with Lin$^-$c-*kit*^{POS}cells, left ventricular (LV) end-diastolic pressure (LVEDP) was 36% lower, and developed pressure (LVDP), LV + dP/dt and LV − dP/dt were 32%, 40% and 41% higher, respectively.

Locally transplanted Lin$^-$c-*kit*^{POS} bone marrow cells have a high capacity for cardiac tissue differentiation. Here, they led to the formation of new myocytes, endothelial cells and smooth muscle cells generating *de novo* myocardium, inclusive of coronary arteries, arterioles and capillaries. The partial repair of the infarcted heart implies that the transplanted cells responded to signals from the injured myocardium that promoted their migration, proliferation and differentiation within the necrotic area of the ventricular wall (Fig. 6b). These differentiating myocytes expressed nuclear and cytoplasmic proteins typical of cardiac tissue. The presence of connexin 43 points to cellular coupling and functional competence of the restored myocardium (Fig. 6b). With postnatal maturation, stem cell function was assumed previously to be restricted to cell lineages present in the organ from which they are derived. However, this limitation in stem cell differentiation potential has been challenged by studies showing that bone marrow and neural stem cells can produce many cell types[4,5,18–20]. We report, for the first time, that a subpopulation of primitive bone marrow cells regenerate myocardium *in vivo*, replacing dead tissue.

Haematopoietic stem cells (HSCs), neural-crest-derived melanoblasts and primordial germ cells express c-*kit* on their cell membrane. These primitive cells migrate during fetal development,

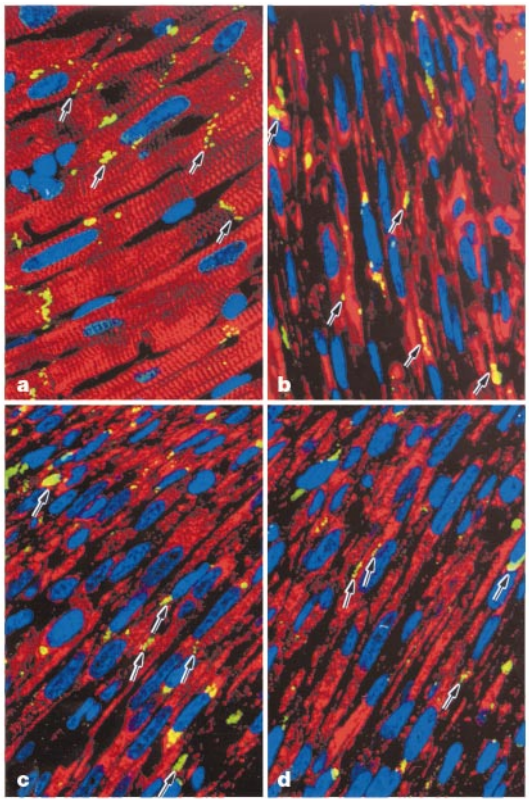

Figure 4 Myocardial repair and connexin 43. **a**, Border zone; **b**–**d**, regenerating myocardium. Shown are connexin 43 (yellow–green; arrows indicate contacts between myocytes) and α-sarcomeric actin (red), and PI-stained nuclei (blue). Original magnification, ×500 (**a**), ×800 (**b**–**d**).

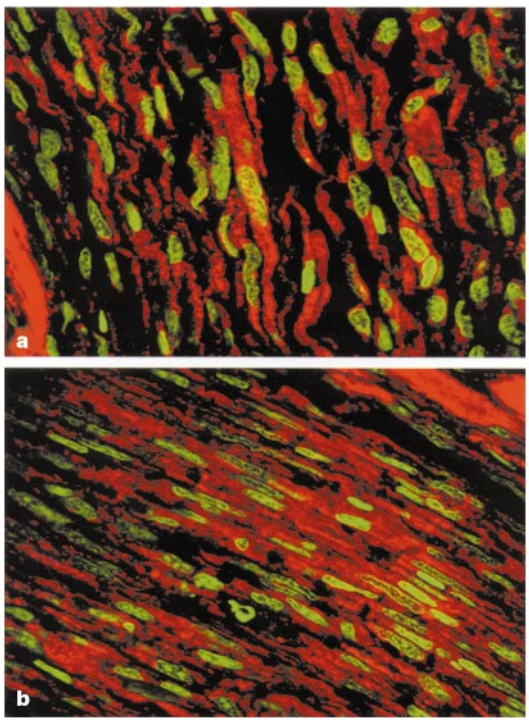

Figure 5 Myocardial infarcts injected with Lin$^-$c-*kit*^{POS} cells: regenerating myocytes. Shown are cardiac myosin (red), and propidium-iodide-labelled nuclei (yellow–green). Original magnification, ×1,000 (**a**); ×700 (**b**).

© 2001 Macmillan Magazines Ltd

homing to the yolk sac and liver. Both of these organs are positive for messenger RNA encoding stem cell factor (SCF), the ligand for c-*kit*[21]. It is thought that membrane-bound SCF mediates the migration of HSC and other primitive cells to their target organs[22]. The fetal and neonatal hearts are positive for SCF transcripts[21] and, although it is not clear whether adult heart cells generate SCF, the c-*kit*/SCF pathway might be the mechanism by which, in our conditions, transplanted Lin$^-$c-*kit*^{POS} cells migrated from the site of injection to the infarcted myocardium.

When a stem cell divides, two daughter cells are formed; these may maintain stem cell properties or become differentiating cells[23] that multiply much more rapidly than stem cells[24]. The Lin$^-$c-*kit*^{POS} cells in these transplants produced the three main cell types of the heart: myocytes constituted the predominant and most active growth component of the regenerating myocardium; endothelial and smooth muscle cells were fast growing but were smaller fractions of the developing tissue. Our observations are difficult to compare with those obtained in the cryo-injured rat heart after injecting cultured myocytes derived from mesenchymal bone marrow cells[25]. Formation of myotubules *in vitro* was required for successful transplantation in that study[25], which contrasts with our results. Cryo-injury has no human counterpart. It constitutes an unusual damage with an intact coronary circulation. This may be why only a few endothelial cells were possibly linked to the original culture system[25] and smooth muscle cells were not detected. Also at variance with our data is the fact that there was no replacement of damaged myocardium with functioning tissue.

Coronary heart disease accounts for 50% of all cardiovascular deaths and nearly 40% of the incidence of heart failure. The current findings have provided compelling evidence that our approach has relevant implications for human disease. Locally delivered primitive bone marrow cells promoted successful treatment of large myocardial infarcts after the completion of ischaemic cell death. This therapeutic intervention reduced the infarcted area and improved cardiac haemodynamics. Infarct size is a major determinant of morbidity and mortality, as massive infarcts affecting 40% or more of the left ventricle in patients are associated with intractable cardiogenic shock or the rapid development of congestive heart failure[1]. In the past, recovery of cardiac function has been fully dependent on the growth of the remaining non-infarcted portion of the ventricle. However, the hypertrophied infarcted heart undergoes progressive deterioration, leading to a dilated myopathy, terminal failure and death[1]. Transplanted Lin$^-$c-*kit*^{POS} bone marrow cells have the capability of regenerating acutely significant amounts of contracting myocardium. This new form of repair can improve the immediate and long-term outcome of ischaemic cardiomyopathy. □

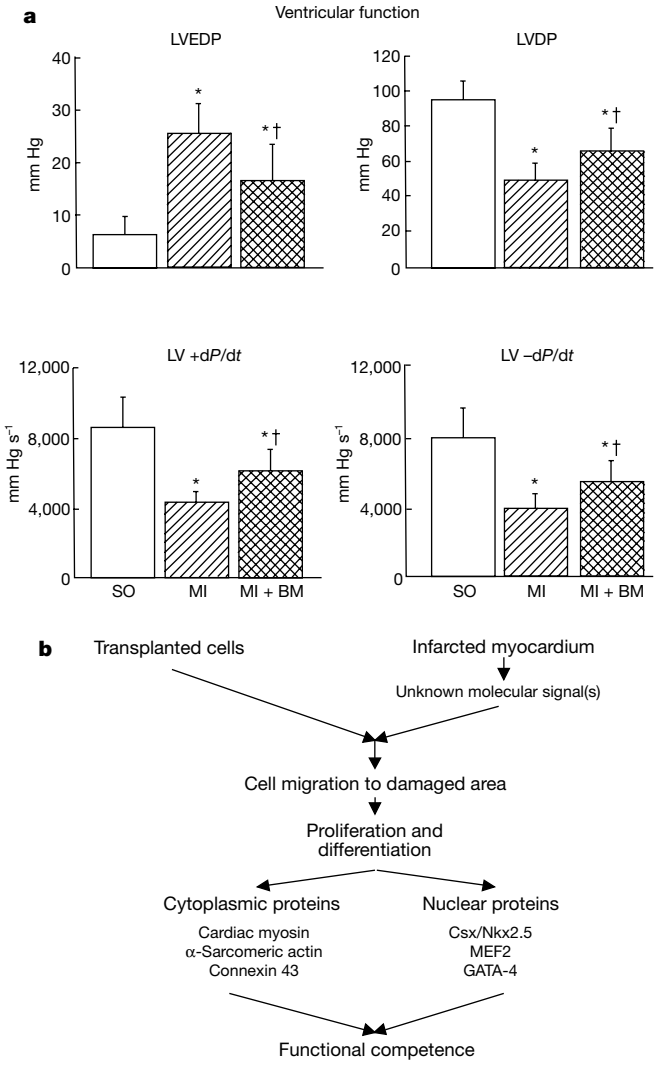

Figure 6 Postulated mechanism of myocardial regeneration and its effect on ventricular function. **a**, Effects of myocardial infarction (MI) on left ventricular end-diastolic pressure (LVEDP), developed pressure (LVDP), LV+ d*P*/d*t* (rate of pressure rise) and LV– d*P*/d*t* (rate of pressure decay). Results are from sham-operated mice (SO, $n = 11$), mice non-injected with Lin$^-$c-*kit*^{POS} cells (MI; $n = 5$ injected with Lin$^-$c-*kit*^{NEG} cells; $n = 6$ non-injected), and mice injected with Lin$^-$c-*kit*^{POS} cells (MI+BM, $n = 9$). Values are mean ± s.d. *$P < 0.05$ versus SO; †$P < 0.05$ versus MI. **b**, Proposed scheme for Lin$^-$c-*kit*^{POS} cell differentiation in cardiac muscle and functional implications.

Methods

Lin$^-$c-*kit*^{POS} cells

We collected bone marrow from the femurs and tibias of male transgenic mice expressing EGFP[9]. Cells were suspended in PBS containing 5% fetal calf serum (FCS) and incubated on ice with rat anti-mouse monoclonal antibodies specific for the following haematopoietic lineages: CD4 and CD8 (T lymphocytes), B-220 (B lymphocytes), Mac-1 (macrophages), GR-1 (granulocytes) (all Caltag Laboratories) and TER-119 (erythrocytes) (Pharmingen). Cells were then rinsed in PBS and incubated for 30 min with magnetic beads coated with goat anti-rat immunoglobulin (Polysciences). Lineage-positive cells were removed by a biomagnet and the 10% remaining lineage-negative (Lin$^-$) cells were stained with ACK-4-biotin (anti-c-*kit* monoclonal antibody). Cells were rinsed in PBS, stained with streptavidin-conjugated phycoerythrin (SA-PE) (Caltag) and sorted by FACS using a FACSVantage instrument (Becton Dickinson). We excited EGFP and ACK-4-biotin-SA-PE at a wavelength of 488 nm. The Lin$^-$ cells were sorted as c-*kit*-positive (c-*kit*^{POS}) and c-*kit*-negative (c-*kit*^{NEG}) with a 1–2 log difference in staining intensity. The c-*kit*^{POS} cells were suspended at a concentration of 3×10^4 to 2×10^5 cells in 5 μl of PBS, and the c-*kit*^{NEG} cells were suspended at a concentration of 5×10^4 to 5×10^5 in 5 μl of PBS[10].

Myocardial infarction

Myocardial infarction was induced in female C57BL/6 mice at 2 months of age as described[11]; 3–5 h after infarction, the thorax was re-opened and 2.5 μl PBS containing Lin$^-$c-*kit*^{POS} cells were injected in the anterior and posterior aspects of the viable myocardium bordering the infarct. Infarcted mice that were not injected or injected with Lin$^-$c-*kit*^{NEG} cells and sham-operated mice were used as controls. All animals were killed 9 ± 2 days after surgery. Protocols were approved by an institutional review board.

Ventricular function

Mice were anaesthetized with chloral hydrate (400 mg per kg (body weight), intraperitoneally (i.p.)), and the right carotid artery was cannulated with a microtip pressure transducer (model SPR-671; Millar) for the measurements of LV pressures, and LV + and LV– d*P*/d*t* in the closed-chest preparation. The abdominal aorta was cannulated, the heart was arrested in diastole, and the myocardium was perfused retrogradely with 10% buffered formalin[11,26]. Three tissue sections, from the base to the apex of the left ventricle, were stained with haematoxylin and eosin. At 9 ± 2 days after coronary occlusion, the infarcted portion of the ventricle was easily identifiable grossly and histologically (see Fig. 1a). The lengths of the endocardial and epicardial surfaces delimiting the infarcted region, and the endocardium and epicardium of the entire left ventricle, were measured in each section. Subsequently, their quotients were computed to yield the average infarct size in each case. This was accomplished at ×4 magnification with an image analyser connected to a microscope[11].

© 2001 Macmillan Magazines Ltd

Cell proliferation and EGFP detection

To establish whether Lin$^-$c-*kit*^{POS} cells resulted in myocardial regeneration, we administered BrdU (50 mg per kg (body weight), i.p.) to the animals daily for 4–5 consecutive days before death. Sections were incubated with anti-BrdU antibody, and BrdU labelling of cardiac cells was measured[17]. Moreover, expression of Ki67 in nuclei was evaluated by treating samples with a rabbit polyclonal anti-mouse Ki67 antibody (Dako). Fluorescein isothiocyanate (FITC)-conjugated goat anti-rabbit IgG was used as secondary antibody. EGFP was detected with a rabbit polyclonal anti-GFP (Molecular Probes). Myocytes were recognized with a mouse monoclonal anti-cardiac myosin heavy chain (MAB 1552; Chemicon) or a mouse monoclonal anti sarcomeric α-actin (clone 5C5; Sigma), endothelial cells with a rabbit polyclonal anti-human factor VIII (Sigma) and smooth muscle cells with a mouse monoclonal anti-smooth-muscle α-actin (clone 1A4; Sigma). Nuclei were stained with propidium iodide, 10 $\mu g\,ml^{-1}$ (refs 27, 28). We determined the percentages of myocyte (M), endothelial cell (EC) and smooth muscle cell (SMC) nuclei labelled by BrdU and Ki67 by confocal microscopy. This was accomplished by dividing the number of nuclei labelled by the total number of nuclei examined. Numbers of nuclei sampled in each cell population were as follows. BrdU labelling: M, 2,908; EC, 2,153; SMC, 4,877. Ki67 labelling: M, 3,771; EC, 4,051; SMC, 4,752. Numbers of cells counted for EGFP labelling: M, 3,278; EC, 2,056; SMC, 1,274. We determined the percentage of myocytes in the regenerating myocardium by delineating the area occupied by cardiac-myosin-stained cells and dividing this by the total area represented by the infarcted region in each case.

Y chromosome

For the fluorescence *in situ* hybridization assay, we exposed sections to a denaturing solution containing 70% formamide. After dehydration with ethanol, sections were hybridized with the DNA probe CEP Y (satellite III) Spectrum Green (Vysis) for 3 h (ref. 29). Nuclei were stained with propidium iodide.

Transcription factors and connexin 43

Sections were incubated with rabbit polyclonal anti-MEF2 (C-21; Santa Cruz), rabbit polyclonal anti-GATA-4 (H-112; Santa Cruz), rabbit polyclonal anti-Csx/Nkx2.5 (obtained from Dr S. Izumo) and rabbit polyclonal anti-connexin 43 (Sigma). We used FITC-conjugated goat anti-rabbit IgG (Sigma) as the secondary antibody[30].

Statistical analysis

Results are presented as means ± s.d. Significance between two measurements was determined by Student's *t*-test, and in multiple comparisons was evaluated by the Bonferroni method. Values of $P < 0.05$ were considered significant.

Received 7 November 2000; accepted 16 February 2001.

1. Pfeffer, M. A. & Braunwald, E. Ventricular remodeling after myocardial infarction. *Circulation* **81,** 1161–1172 (1990).
2. Ferrari, G. *et al.* Muscle regeneration by bone marrow-derived myogenic progenitors. *Science* **279,** 1528–1530 (1998).
3. Jackson, K. A., Mi, T. & Goodell, M. A. Hematopoietic potential of stem cells isolated from murine skeletal muscle. *Proc. Natl Acad. Sci. USA* **96,** 14482–14486 (1999).
4. Eglitis, M. A. & Mezey, E. Hematopoietic cells differentiate into both microglia and macroglia in the brains of adult mice. *Proc. Natl Acad. Sci. USA* **94,** 4080–4085 (1997).
5. Theise, N. D. *et al.* Liver from bone marrow in humans. *Hepatology* **32,** 11–16 (2000).
6. Brazelton, T. A., Rossi, F. M. V., Keshet, G. I. & Blau, H. M. From marrow to brain: expression of neuronal phenotypes in adult mice. *Science* **290,** 1775–1779 (2000).
7. Mezey, E., Chandross, K. J., Harta, G., Maki, R. A. & McKercher, S. R. Turning blood into brain: cells bearing neuronal antigens generated in vivo from bone marrow. *Science* **290,** 1779–1782 (2000).
8. Vogel, G. Stem cells: new excitements, persistent questions. *Science* **290,** 1672–1674 (2000).
9. Hadjantonakis, A. K., Gerstenstein, M., Ikawa, M., Okabe, M. & Nagy, A. Generating green fluorescent mice by germline transmission of green fluorescent ES cells. *Mech. Dev.* **76,** 79–90 (1998).
10. Orlic, D., Fischer, R., Nishikawa, S.-I., Nienhuis, A. W. & Bodine, D. M. Purification and characterization of heterogeneous pluripotent hematopoietic stem cell populations expressing high levels of c-*kit* receptor. *Blood* **82,** 762–770 (1993).
11. Li, Q. *et al.* Overexpression of insulin-like growth factor-1 in mice protects from myocyte death after infarction, attenuating ventricular dilation, wall stress, and cardiac hypertrophy. *J. Clin. Invest.* **100,** 1991–1999 (1997).
12. Durocher, D., Charron, F., Warren, R., Schwartz, R. J. & Nemer, M. The cardiac transciption factors Nkx2-5 and GATA-4 are mutual cofactors. *EMBO J.* **16,** 5687–5696 (1997).
13. Morin, S., Charron, F., Robitaille, L. & Nemer, M. GATA-dependent recruitment of MEF2 proteins to target promoters. *EMBO J.* **19,** 2046–2055 (2000).
14. Beardsle, M. A., Laing, J. G., Beyer, E. C. & Saffitz, J. E. Rapid turnover of connexin43 in the adult rat heart. *Circ. Res.* **83,** 629–635 (1998).
15. Musil, L. S., Le, A. N., VanSlyke, J. K. & Roberts, L. M. Regulation of connexin degradation as a mechanism to increase gap junction assembly and function. *J. Biol. Chem.* **275,** 25207–25215 (2000).
16. Scholzen, T. & Gerdes, J. The ki-67 protein: from the known and the unknown. *J. Cell. Physiol.* **182,** 311–322 (2000).
17. Kajstura, J. *et al.* Myocyte cellular hyperplasia and myocyte cellular hypertrophy contribute to chronic ventricular remodeling in coronary artery narrowing-induced cardiomyopathy in rats. *Circ. Res.* **74,** 383–400 (1994).
18. Clarke, D. L. Generalized potential of adult neural stem cells. *Science* **288,** 1660–1663 (2000).
19. Theise, N. D. *et al.* Derivation of hepatocytes from bone marrow cells in mice after radiation-induced myeloablation. *Hepatology* **31,** 235–240 (2000).
20. Lagasse, E. *et al.* Purified hematopoietic stem cells can differentiate into hepatocytes *in vivo*. *Nature Med.* **6,** 1229–1234 (2000).
21. Kunisada, T. *et al.* Transgene expression of steel factor in the basal layer of epidermis promotes survival, proliferation, differentiation and migration of melanocyte precursors. *Development* **125,** 2915–2923 (1998).
22. Matsui, Y., Zsebo, K. M. & Hogan, B. Embryonic expression of a haematopoietic growth factor encoded by the S1 locus and the ligand for c-kit. *Nature* **347,** 667–669 (1990).
23. Morrison, S. J., Uchida, N. & Weissman, I. L. The biology of hematopoietic stem cells. *Annu. Rev. Cell Dev. Biol.* **11,** 35–71 (1994).
24. Morrison, S. J., Shah, N. M. & Anderson, D. J. Regulatory mechanisms in stem cell biology. *Cell* **88,** 287–298 (1997).
25. Tomita, S. *et al.* Autologous transplantation of bone marrow cells improves damaged heart function. *Circulation* **100** (Suppl.), II-247–II-256 (1999).
26. Li, B. *et al.* Insulin-like growth factor-1 attenuates the detrimental impact of non occlusive coronary artery constriction on the heart. *Circ. Res.* **84,** 1007–1019 (1999).
27. Leri, A. *et al.* Stretch-mediated release of angiotensin II induces myocyte apoptosis by activating p53 that enhances the local renin-angiotensin system and decreases the Bcl-2-to-Bax protein ratio in the cell. *J. Clin. Invest.* **101,** 1326–1342 (1998).
28. Kajstura, J. *et al.* Myocyte proliferation in end-stage cardiac failure in humans. *Proc. Natl Acad. Sci. USA* **95,** 8801–8805 (1998).
29. Kajstura, J. *et al.* Telomere shortening is an *in vivo* marker of myocyte replication and aging. *Am. J. Pathol.* **156,** 813–819 (2000).
30. Leri, A. *et al.* Pacing-induced heart failure in dogs enhances the expression of p53 and p53-dependent genes in ventricular myocytes. *Circulation* **97,** 194–203 (1998).

Supplementary information is available on *Nature*'s World-Wide Web site (http://www.nature.com) or as paper copy from the London editorial office of *Nature*.

Acknowledgements

We thank Dr S. Izumo for providing us with the Csx2.5 antibody. This work was supported by grants from the NIH. S.C. is supported by a fellowship from the Mario Negri Institute of Pharmacologic Research, Milan, Italy.

Correspondence and requests for materials should be addressed to P.A. (e-mail: piero_anversa@nymc.edu).

CaT1 manifests the pore properties of the calcium-release-activated calcium channel

Lixia Yue*, Ji-Bin Peng†, Matthias A. Hediger† & David E. Clapham*‡

‡ *Howard Hughes Medical Institute and * Children's Hospital, Harvard Medical School, Enders 1309, 320 Longwood Avenue, Boston, Massachusetts 02115, USA*
† *Membrane Biology Program and Renal Division, Brigham and Women's Hospital and Harvard Medical School, Boston, Massachusetts 02115, USA*

The calcium-release-activated Ca^{2+}channel, I_{CRAC}[1–3], is a highly Ca^{2+}-selective ion channel that is activated on depletion of either intracellular Ca^{2+} levels or intracellular Ca^{2+} stores. The unique gating of I_{CRAC} has made it a favourite target of investigation for new signal transduction mechanisms; however, without molecular identification of the channel protein, such studies have been inconclusive. Here we show that the protein CaT1 (ref. 4), which has six membrane-spanning domains, exhibits the unique biophysical properties of I_{CRAC} when expressed in mammalian cells. Like I_{CRAC}, expressed CaT1 protein is Ca^{2+} selective, activated by a reduction in intracellular Ca^{2+} concentration, and inactivated by higher intracellular concentrations of Ca^{2+}. The channel is indistinguishable from I_{CRAC} in the following features: sequence of selectivity to divalent cations; an anomalous mole fraction effect; whole-cell current kinetics; block by lanthanum; loss of selectivity in the absence of divalent cations; and single-channel conductance to Na^+ in divalent-ion-free conditions. CaT1 is activated by both passive and active depletion of calcium stores. We propose that CaT1 comprises all or part of the I_{CRAC} pore.

© 2001 Macmillan Magazines Ltd